Effects of Various Geometric Parameters on Flow Behavior in Sonic Nozzles

E. von Lavante [1], A. Zachcial [1], D. Zeitz [1], B. Nath [2], H. Dietrich [2]
[1] *University of Essen, Germany*
[2] *ELSTER Production GmbH, Germany*

Abstract: Numerical analysis of flow fields associated with sonic Venturi nozzles with various modifications of its basic geometry was carried out. The baseline nozzle, used for gas flow metering, was simulated at Reynolds number $1.5 \cdot 10^5$. The modifications included a backward facing step in the nozzle wall just after the throat, suction through the wall and three different diffuser opening angles. The flow was simulated using compressible viscous flow solver ACHIEVE developed by the authors. In some cases, a noticable improvement in the flowrate and, consequently, increase in the discharge coefficient C_d was achieved

Keywords: Critical Nozzles, Discharge Coefficient, Numerical Simulation, Boundary Layer Control, Boundary Layer Suction

1 Introduction

One of the simplest methods of highly accurate measurement of mass flows is by means of critical venturi nozzles. As a matter of fact, sonic nozzle test rigs are often used as reference flow meters. The guidelines and standards in using these devices are well defined and covered by the ISO Standard 9300 [1]. It is valid for relatively large and medium size nozzles, with mass flows down to a minimum of $33\,m^3/h$ and Reynolds numbers of approximately $Re_{ISO} = 10^5$. However, recent investigations (von Lavante et al. [3]) indicate that at the lower end of the Reynolds number range recommanded by the ISO standard [1] and high pressure ratio between the outflow pressure and the stagnation pressure p_{out}/p_0 unsteady phenomena could occure, leading to a slight decrease of the discharge coefficient C_d. The reason for this behavior is strong interaction between unsteady upstream traveling shocks and downstream convected vortices produced by intermittent boundary layer separation. These pressure waves can lead to a partial "unchoking" of the flow in the the throat and are, therefore, undesired for flow metering.

One possibility to try to avoid the above effects is to modify the geometry of the nozzle. Several investigators have conducted experiments with modified nozzles differing somewhat from the ISO standard. Pereira et al. [9] have measured the C_d coefficient in toroidal nozzles with steps between the throat and diffuser. The steps were either "positive" (backward facing, causing expansion) or "negative" (forward facing, causing compression). Their main purpose was easier manufacturing, though, not more favourable flow conditions. Dudzinsky et al. [10] have considered cylindrical Venturi nozzles with steps immediately after the cylindrical part of the nozzle. Their results are not indicative of any changes in the flow rate. Williamson et al. [11] investigated several nozzle shapes at sonic and subsonic conditions. They measured the static pressure through a pressure tap located just after the backward facing step. In the sonic case, the measured pressure revealed strong expansion around the step.

The aim of the present research is to investigate the influence of several geometrical parameters on the nozzle flow in general and its flow metering performance in particular. The main hope of the present study, carried out numerically, was to find a nozzle shape that would minimize the above

negative effects at Reynolds number $Re_{ISO} = 1.5 \cdot 10^5$.

2 Numerical Algorithm

The numerical method employed in the present flow simulations is part of a flow simulation system developed at the Institute of Turbomachinery at the University of Essen, called "ACHIEVE". It consists of an upwind solver of the Navier-Stokes equations, using the finite volume discretization. The governing equations to be solved in the present simulations are the two-dimensional or axisymmetric compressible Navier-Stokes equations. In the two-dimensional case, they are, in a simplified vector form in general, body-fitted coordinates ξ and η in the weak conservation law form:

$$\frac{\partial Q_{2-D}}{\partial \tau} + \frac{\partial (F_{2-D} - F_{v,2-D})}{\partial \xi} + \frac{\partial (G_{2-D} - G_{v,2-D})}{\partial \eta} = 0 \qquad (1)$$

with $Q_{2-D} = J^{-1}(\rho, \quad \rho u, \quad \rho v, \quad e)^T$ the vector of the conserved variables. J is the Jacobian of the coordinates transformation from physical (x, y, t) to computational (ξ, η, τ) space. It is given for a stationary computational grid as $J^{-1} = x_\xi y_\eta - y_\xi x_\eta$. The inviscid flux vector F_{2-D} and the viscous flux vector footnotesize $F_{v,2-D}$ in, for example, the ξ direction can be found in Here, footnotesize $F_{v,2-D}$ contains the components of the shear-stress tensor and q_i, the heat-flux vector, is obtained using Fourier's law. The expressions for all the fluxes, including G_{2-D} and $G_{v,2-D}$, are given by, for example, Steger [6] or von Lavante and Groenner [2] and will not be repeated here. The axisymmetric form of the governing equations is similar:

$$\frac{\partial Q_{ax}}{\partial \tau} + \frac{\partial (F_{ax} - F_{v,ax})}{\partial \xi} + \frac{\partial (G_{ax} - G_{v,ax})}{\partial \eta} + \frac{H}{J} = 0 \qquad (2)$$

where $Q_{ax} = y\, Q_{2-D}$, $F_{ax} = y\, F_{2-D}$, $F_{v,ax} = y\, F_{v,2-D}$, $G_{ax} = y\, G_{2-D}$, and $G_{v,ax} = y\, G_{v,2-D}$. The source term H is $H = -(0, \quad 0, \quad p - \tau_{\Theta\Theta}, \quad 0)^T$, with $\tau_{\Theta\Theta} = \frac{2}{3}\, \mu\, (2\frac{v}{y} - \frac{\partial v}{\partial y} - \frac{\partial u}{\partial x})$. The governing equations are given in more detail by, for example, Steger [6] or von Lavante et. al. [5].

2.1 Numerical Scheme

Due to the complexity of the predicted flow, a simple numerical scheme with central spacial differences and artificial dissipation added explicitely was not suited for the present simulations. Therefore, the well known and proven Roe's Scheme [2] was employed. The numerical scheme is based on Roe's Flux Difference Splitting in finite volume form, as developed by von Lavante et. al. [5]. The method has been proven to be accurate and effective in the simulation of viscous flows with wide range of Mach numbers [2].

The reconstruction of the cell-centered variables to the cell-interface locations for the computation of convective terms was done using a monotone interpolation of the primitive variables $Q_p = (\rho,\ u,\ v,\ p)^T$. The interpolation slope was limited by an appropriate limiter, according to the previously published MUSCL type procedure (see, for example, [5]).
In the present work, the second order accurate upwind biased Fromm scheme ($\kappa = 0$) and the van Albada form of the limiter has been used. The viscous fluxes F_v and G_v were centrally differenced.

2.2 Discretization in Time

The governing equations were integrated in time by solving their semidiscrete form by means of either modified Runge-Kutta (R-K) time stepping or implicit symmetric Gauß-Seidel (SGS) relaxation method. In the present work, the two stage version of the R-K procedure was utilized. The

corresponding Runge-Kutta coefficients α_i were optimized by von Lavante et. al. [7] for maximum multigrid performance (damping of high frequencies). That optimization was done, however, using a linear hyperbolic model equations. In realistic applications, these coefficients worked fine for the inviscid Euler equations as well as for most viscous cases. The simple two stage R-K procedure was as efficient as the more frequently used four stage scheme, but required only one optimized coefficient, $\alpha_1 = 0.42$.

The simulations were carried out on structured grids. The mesh points were arranged according to an algebraic distribution and clustered at the solid walls to ensure enough gridpoints in the boundary layers. The domain was divided into several blocks to make the formulation of the boundary conditions and handling a complex geometry easier. Furthermore, the Multiblock-structure was necessary to compute the flow on parallel computers.

2.3 Boundary Conditions

The present boundary conditions were implemented with the help of dummy (ghost) cells. At the subsonic inflow boundary, a locally one-dimensional weakly non-reflective boundary condition, based on the isentropic theory of the Riemann problem, was used. The tangetial velocity, incoming Riemann invariant, total pressure and entropy in the first ghost cell were specified. The outgoing Riemann invariant was extrapolated from the interior domain. At the subsonic outflow boundary, the static pressure was specified, subject to the fluctuations allowed by the non-reflective treatment. The remaining variables were extrapolated. At solid walls, the velocities were anti-reflected, resulting in zero velocity on the boundary. The static pressure and density were reflected, resulting in zero gradients of these variables at the wall (adiabatic wall). Finally, at the interzonal boundaries, the block grids were overlapping by two cells, providing smooth transitions of the dependant variables Q due to the present MUSCL extrapolation in the projection phase.

2.4 Varification and Validation

The present numerical algorithm was subjected to verification of it's temporal and spatial accuracy and consistancy. The scheme is formally second order accurate in space, since the viscous terms are obtained from second order central differences. The scheme was first verified using the usual grid refinement study for the case of viscous flat plate flow at a free stream Mach number of $M_\infty = 0.5$. Defining the global error as the L_2 - norm of the deviation of the present solution from the Blasius solution, second order accuracy was verified (von Lavante [7]). The temporal accuracy was tested by simulating the 2-D flow about a cylinder, with free stream Mach number $M_\infty = 0.1$ and a Reynolds number of Re $= 200$. The resulting Strouhal number of the vortex separation was compared with known experimental and numerical results, see Table 1. The agreement was certainly acceptable.

	Method	Strouhal num.
Lugt	experimental	0.193
Truckenbrodt	experimental	0.192
Authors	numerical	0.190

Table 1. Strouhal number in cylinder wake flow.

3 Results

A representative critical nozzle geometry, as recommended by the ISO Standard 9300 [1] was selected for the base line investigations. The nozzle shape is shown in Fig. 1. It is a typical convergent-divergent nozzle, with a throat diameter of 10 mm, and a divergent part of 70 mm length, having a divergence wall angle of 4^o. The nozzle was manufactured out of stainless steel and was intensively tested. In this work, only air as working fluid was considered. The flow into the nozzle was entering at atmospheric conditions, with the total temperature $T_0 = 293.14\,K$ and total pressure $P_0 = 1013.25\,mbar$. The back pressure ratio in the nozzle was varied, $p_{out}/p_0 = 0.5 - 0.8$. The Reynolds number was in this case $Re_{ISO} = 1.5 \cdot 10^5$.

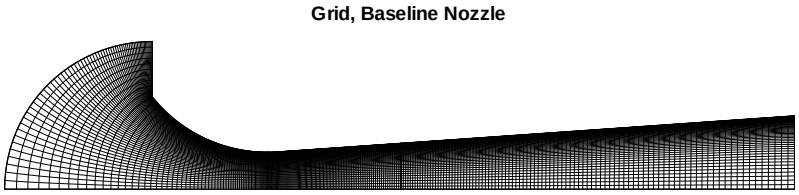

Figure 1: Computational grid consisting of two blocks.

According to the real physics of the flow, the nozzle was started from zero flow condition (quiescent), the velocity being induced by the low pressure at the end of the nozzle. The highest back pressure ratio was too large to result in smooth supersonic flow in the entire nozzle. A system of complex shock waves was induced, causing periodic flow separation at the wall. The separated bubbles detached from the wall and formed vorticies that were convected downstream. The separated boundary layer had a noticeble blockage effect, causing a highly fluctuating flow at the outflow and, more seriously, in the throat.
Therefore, the nozzle geometry was modified in order to ensure smoother flow. Following three cases will discussed in this paper:
1. Variation of the diffusor opening angle α_d
3. Backward facing step just after the throat
4. Boundary layer suction downstream of the throat

3.1 Diffuser opening angle α_d

According to the ISO 9300-standard [1], the toroidal nozzle diffusor should have an opening angle between $\alpha_d = 2.5^o - 6.0^o$. In the present work, four discrete angles were simulated: $\alpha_d = 2.5^o, 3.0^o, 4.0^o$ and 5.0^o. Table 2 summerizes the resulting discharge coefficient C_d as compared to the experimentally determined value for back pressure ratio $p_{out}/p_0 = 0.6$.

Experiment	2.5^o	3.0^o	4.0^o	5.0^o
0.985	0.986	0.987	0.989	0.981

Table 2. Comparison of discharge coefficients for different diffuser opening angles.

Obviously, at least as far as the present simulation is concerned, the diffuser opening angle has very small influence on the resulting flow rate, as far as the angle α_d is within the limits set by [1]. It

seems that the optimal angle α_d is approximately 4.0 degrees.

3.2 Backward facing step

Taking into consideration the results of previous work by various investigators, it was decided to simulate the flow in a nozzle with a small backward facing step placed just after the throat. The step produces fairly strong expansion wave system that interacts with possible upstream traveling waves, making them much weaker and possibly preventing them from continuing on into the throat. The back pressure ratio was in this case $p_{out}/p_0 = 0.8$, resulting in periodic unchoking in the baseline case (without the step). The step was at x=0, immediately after the throat. It was 0.25 mm high ($\frac{\Delta y}{D^*} = 0.025 = 2.5\%$). The resulting velocity vectors and Mach contours can be seen in Fig. 2.

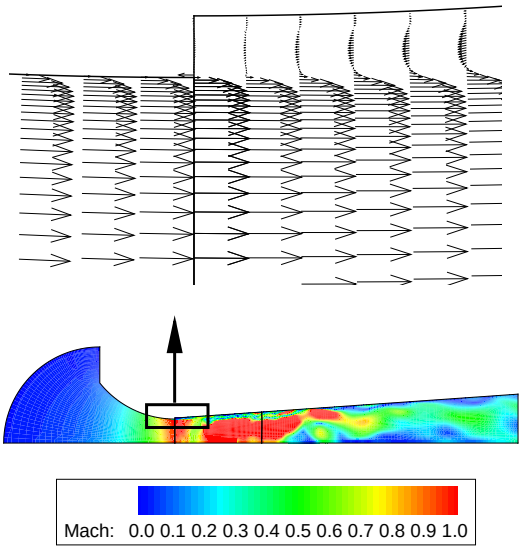

Figure 2: Velocity vectors at the step.

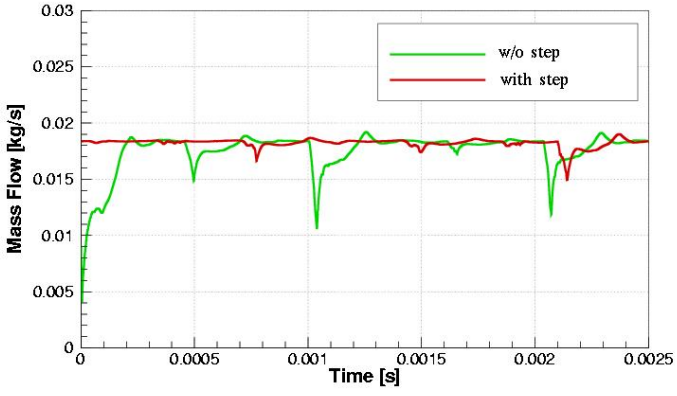

Figure 3: Comparison of massflow rates with and without step.

The introduction of the step improved the flow behavior markedly, resulting in higher value of the

discharge coefficient C_d. The comparison of timewise history of C_d for the nozzles with and without the step can be seen in Fig. 3.
The pressure waves encountered in the nozzle with the step are much weaker than in the baseline nozzle. This is reflected in an improvement of the integral value of C_d (time averaged): 0.975 with step vs. 0.954 without.

3.3 Boundary layer suction

Boundary layer blowing and suction are common methods in external aerodynamics to locally accelarate fluid in a boundary layer, thus delaying possible separation. Blowing is not applicable in this case, since it would introduce additional massflow, but suction would be possible if the fluid being removed is fed back into the main stream. In the present work, several different suction locations and rates were tested. Best results were obtained for the combination shown in Fig. 4. Here, two slits were located at x=1.75mm and x=3.75mm downstream of the throat. The width was in both cases 0.5mm. Assuming critical flow in the slits, the massflow being sucked out amounted to $\dot{m}_{suc} = \dot{m}_{tot} \cdot 0.002$, or with other words 0.2% of the main flow.

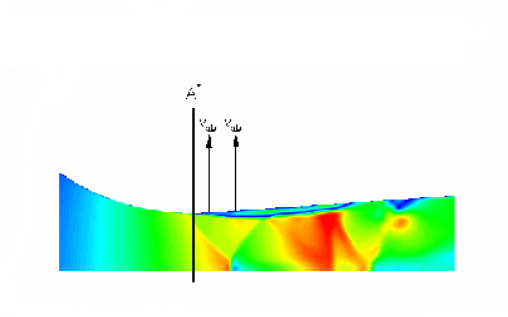

Figure 4: Location of the suction slits on Mach number contours.

The local streamlines at the suction openings are displayed in Fig. 5, together with total velocity contours (isotachs).

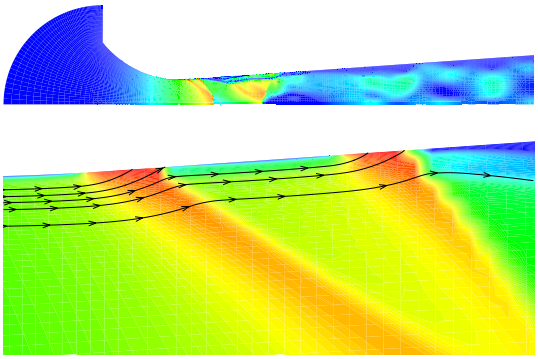

Figure 5: Streamlines and constant velocity contours.

The suction had a dramatic effect on the flow in the boundary layer. With the suction in effect, the boundary layer was attached, almost totally eliminating the local unsteady flow behavior. This, again, has a significant influence on the flow rate. As can be seen in Fig. 6, the discharge coefficient

C_d is absolutely constant, indicating that no disturbances are present in the throat.

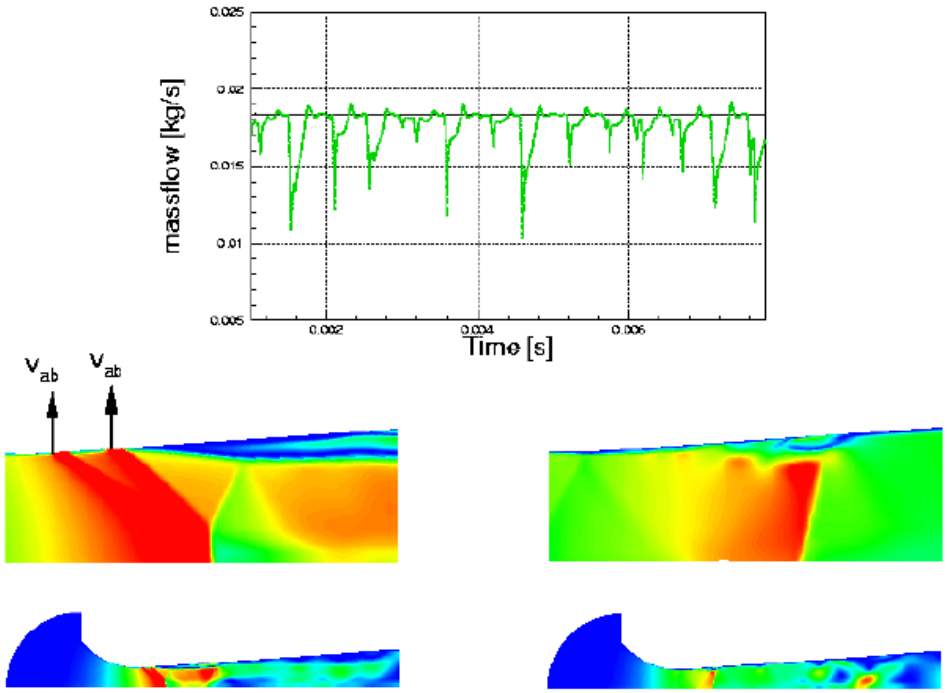

Figure 6: Comparison of massflow rates with and without suction.

4 Conclusions

Several possible modifications of the basic geometry of sonic Venturi nozzles were investigated. Best results were achieved by using active boundary layer controll. The practical implementation of boundary layer suction is, however, at the best difficult and may not be of practical significance. The introduction of a small backward facing step seems to be promissing and should be further investigated.

[1] International Standard ISO 9300, "Measurement of gas flow by means of critical flow Venturi nozzles", First Edition, Beuth, Berlin 1990.

[2] von Lavante, E. and Grönner, J., "Semiimplicit Schemes for Solving the Navier-Stokes Equations", 9th GAMM Conference, Lausanne, Notes on Numerical Fluid Mechanics, Vieweg, 1992.

[3] von Lavante, E., Nath, B. and Dietrich, H., "Effects of Instabilities on Flow Rates in Small Sonic Nozzles", Proceedings of the 9th Int. Conference on Flow Measurement FLOMEKO'98, Lund, 1998.

[4] Ishibashi, M., von Lavante, E. and Takamoto, M., "Quasi- Nonintrusive Measurement of Flow Velocity Field in a Critical Nozzle", Proceedings of ASME FEDSM'00, June 11-15, Boston, 2000.

[5] von Lavante, E., El-Milligui, A. and Warda, H., "Simulation of Unsteady Flows Using Personal Computers", The 3rd Int. Congress on Fluid Mechanics, Cairo, 1990.

[6] Steger, J. L., "Implicit, Finite-Difference Simulation of Flow about Arbitrary Geometries", AIAA Journal, Vol. 16, No. 7, 1978.

[7] von Lavante, E., El-Miligui, A., Cannizzaro, F. E., and Warda, H. A., "Simple Explicit Upwind Schemes for Solving Compressible Flows", Proceedings of the 8th GAMM Conference on Numerical Methods in Fluid Mechanics, Delft, 1990.

[8] Ishibashi, M. and Takamoto, M., "Very Accurate Analytical Calculation of the Discharge Coefficient of Critical Venturi Nozzles with Laminar Boundary Layer", Proceedings of the FLUCOME97, Hayama, Japan, Sept. 1997.

[9] Pereira, M. T., Taira, N. M. and de Mattos Pimenta, M., "Flow Metering With a Modified Sonic Nozzle", Proceedings of the 6th FLOMEKO Conference, Seoul, Oct. 1993.

[10] Dudzinsky, T. J., Johnson, R. C. and Krause L. N., "Venturi Meter with Separable Diffuser", Journal of Basic Engineering, March 1969.

[11] Williamson, L. D., Sawchuk, B. D. and Karnik, U., "The NOVA Meter Prover", 3rd Int. Symposium on Fluid Flow Measurement, San Antonio, March 1995.

AUTHOR(S): Prof. Dr.-Ing. Ernst von Lavante, Institute of Turbomachinery, University of Essen, 45127 Essen, Germany. E-mail: erni@tigger.turbo.uni-essen.de.
Dr. B. Nath, ELSTER Production GmbH, Steinernstr. 19 - 21, 55252 Mainz-Kastel, Germany. E-mail: Burger.Nath@elster.com.